energies

Article

Simulation and Design of a Balanced-Field Electromagnetic Technique Sensor for Crack Detection in Long-Distance Oil and Gas Pipelines

Lijian Yang, Jiayin Li, Wenxue Zheng * and Bin Liu

School of Information Science and Engineering, Shenyang University of Technology, Shenyang 110870, China; yanglijian888@sut.edu.cn (L.Y.); lijiayin@smail.sut.edu.cn (J.L.); liubinsgd@sut.edu.cn (B.L.)
* Correspondence: zh15940011365@sut.edu.cn; Tel.: +86-188-4257-6897

Abstract: Due to the extremely small size and arbitrary orientation of the cracks, a highly sensitive sensor based on the balanced-field electromagnetic technique was designed for in-line inspection of oil and gas pipeline cracks. A balanced-field electromagnetic technique sensor mutual inductance model was established and used to theoretically analyze the parameters affecting sensitivity. Finite element simulation was used to analyze the specific effects of the magnetically conductive medium, the number of coil turns, and the sensor lift-off height on the sensor output, respectively, and the sensor parameters of high sensitivity were determined. The detection effect of the sensor on the pipeline crack was tested by the single-sensor experiment and the pulling test. The results show that the designed balanced-field electromagnetic technique sensor is effective in detecting both circumferential and axial cracks of 0.5 to 6 mm in depth. As the crack depth increases, the sensitivity decreases and the detection voltage amplitude increases linearly. The sensitivity of the sensor is highest when detecting circumferential and axial cracks of 1 mm in depth at 1.76 and 0.87 mV/mm, respectively. In addition, the amplitude of the circumferential crack signal at the same depth is approximately twice that of the axial crack signal.

Keywords: long-distance oil and gas pipelines; balanced-field electromagnetic technique; crack detection; sensor design; sensitivity

check for updates

Citation: Yang, L.; Li, J.; Zheng, W.; Liu, B. Simulation and Design of a Balanced-Field Electromagnetic Technique Sensor for Crack Detection in Long-Distance Oil and Gas Pipelines. *Energies* **2022**, *15*, 5274. https://doi.org/10.3390/en15145274

Academic Editors: Songling Huang, Xiaochun Song and Lisha Peng

Received: 13 June 2022
Accepted: 19 July 2022
Published: 20 July 2022

1. Introduction

With the increase in consumption of oil and natural gas, oil and gas pipelines, as the most important transportation medium in various countries and regions, are also expanding their laying scale [1]. During the service process, the internal and external walls of the pipeline will inevitably suffer from corrosion, deformation, and even cracking due to tensile loads, geographical environment, the corrosiveness of the transported medium, natural aging of the main body of the pipeline, and other factors [2–4]. Among them, cracks play a decisive role in the fracture of the pipeline, seriously affecting the performance and reliability of oil and gas pipelines [5,6]. Because of the high risk of oil and gas, if a pipeline leaks, oil and gas will spread quickly and may even create catastrophic accidents such as explosions, causing not only massive economic losses but also a significant risk to personal safety and the environment. Therefore, effective detection of pipeline cracks can reduce the risk of oil and gas leaks and ensure the smooth operation of pipelines.

In-line inspection (ILI) technology is an effective means to discover pipeline defects and eliminate potential accident hazards at present [7]. The pipeline inspection gauge (PIG) is the most mainstream of the ILI methods. It is driven forward by the pressure difference of the pipeline transport medium. The main detection techniques currently used in PIG are magnetic flux leakage, ultrasonic inspection technique, and eddy current testing [8,9]. Among them, the most mainstream is the magnetic flux leakage detection technology, which has mature applications in the field of pipeline detection and has good detection capabilities for metal loss, pitting, holes, and other defects with a certain volume. However, due to the limitation of the detection principle, it is difficult to detect defects such as cracks with extremely small opening widths [10,11]. Ultrasonic inspection techniques can effectively detect cracks and have high detection accuracy. However, traditional ultrasonic inspection is mostly used for liquid media pipelines due to the limitations of the couplant [12,13]. Electromagnetic non-destructive testing technology is one of the main exploration technologies in the field of crack detection because of its non-contact and wide application environment. Varied detection techniques have different application ranges because of the variety of crack directions and complicated shapes. For example, in terms of electromagnetic ultrasonic, Yang et al. designed an electromagnetic ultrasound transducer capable of simultaneously detecting circumferential and axial cracks in pipelines, and analyzed the relationship between the structure of the grid coil and the biaxial crack detection capability, effectively improving the efficiency of crack detection [14]. Nakamura et al. developed a point-focused electromagnetic ultrasonic transducer. They determined the optimal excitation frequency for generating SV waves, and realized the detection of tiny cracks near steel pipe welds [15]. However, in practical pipeline applications, the detection speed is often controlled at approximately 2 m/s due to the difference between the speed of sound and the speed of electromagnetic waves [16]. Eddy current testing has a high degree of maturity in crack detection, yet traditional eddy current detection techniques are only effective for surface and near surface cracks [17]. In order to increase the detection depth and expand the range of applications, techniques such as a pulsed eddy current [18] and a remote field eddy current [19] have been proposed, but the lift-off effect greatly affects the signal-to-noise ratio and detection accuracy of eddy current detection signals [20]. In addition to the above technologies applied to PIG, alternating current field measurement (ACFM) technique is also well suited to the detection of cracks. However, the single structure ACFM sensor is mainly suitable for axial crack detection [21]. To reduce the blind spot in practical detection, multi-directional crack detection has been achieved in the form of changing the excitation structure or array of magnetoresistive sensors [22–24]. However, due to the structure's intricacy, its application has certain limitations in the field of detection in long-distance oil and gas pipelines. In summary, it is still necessary to explore an engineering applicable method for in-line internal inspection of cracks in long-distance oil and gas pipelines due to the random location and arbitrary direction.

The balanced-field electromagnetic technique is an emerging electromagnetic non-destructive testing technology, which has the advantages of no coupling medium, arbitrary to the detection direction and self-zeroing, and shows good applicability in the detection of pipeline cracks. TESTEX (USA) has developed a balanced-field electromagnetic technique crack detection system that enables the detection of cracks no more than 3.2 mm from the surface, but the detection speed is limited to 0.3 m/s and is only used for off-line external inspection. This off-line and extremely low-speed method is not suitable for full line inspection because long-distance oil and gas pipelines are laid over long distances and buried underground. In addition to this, no published research on the balanced-field electromagnetic technique has been seen. The author has studied the crack detection principle and signal generation process of the balanced-field electromagnetic technique in the early stage. The combination of theory and experiment proves the feasibility of balanced electromagnetic technology to detect cracks at any angle in pipelines [25,26]. However, the extremely small size of the crack has high requirements on the sensitivity of the sensor in practical pipeline detection. In addition, to ensure the effectiveness of the detection, the sensor should have a variable output response to different sizes of cracks while the sensitivity increases, and at the same time, a good correspondence between crack and output can provide a basis for quantifying the crack size. Therefore, the optimization of the sensor sensitivity of the balanced-field electromagnetic technique is of great significance to further evaluate the detection ability of the balanced-field electromagnetic technique, so that it can be more perfect in practical applications.

In this paper, a high-sensitivity balanced-field electromagnetic sensor is designed to meet the needs of in-line inspection of cracks in long-distance oil and gas pipelines and the requirements of crack size on sensor sensitivity, providing a feasible and effective method for in-line inspection of cracks in arbitrary directions in long-distance oil and gas pipelines. Firstly, the relationship between the sensor and pipeline is equated through the establishment of a balanced-field electromagnetic technique mutual inductance model. The parameters affecting the sensitivity of the sensor are analyzed using this model. Secondly, the relationship between the sensor parameters and detection voltage is specifically investigated through finite element simulation using a control variable approach and determines the structural parameters of the highly sensitive sensor. Finally, the sensor's output response to crack depth is used as a judging index to experimentally verify the designed sensor's detection effect. The linear output relationship between the sensor for circumferential and axial cracks is obtained to serve as a foundation for further crack quantification. Moreover, the sensitivity curves are obtained of the designed sensor for circumferential and axial cracks and determine the high-sensitivity characteristics and detection capability of the sensor for smaller-depth cracks. Additionally, the ability of the designed sensor to detect circumferential and axial cracks in practical applications has been demonstrated in PIG pulling testing.

2. Detection Principle and Sensor Parameter Analysis

2.1. The Balanced-Field Electromagnetic Technique Detection Principle

The balanced-field electromagnetic technique is an AC excitation detection method. It uses a pair of mutually orthogonal and spatially geometrically symmetrical coils to generate an alternating magnetic field and an eddy current field on the surface of the pipeline, enabling the detection of crack defects by sensing the electromagnetic changes on the surface of the pipeline [26]. As shown in Figure 1a, when there is no defect on the surface of the pipeline, the magnetic flux directly below the excitation coil varies with the direction of the excitation current and always flows parallel to the surface of the pipeline (XY plane) and does not pass through the detection coil. The changing flux generates an induced current on the surface of the pipeline symmetrical about the detection coil, i.e., the induced currents are equal in size and opposite in direction on both sides of the detection coil. The amount of induced flux into and out of the detection coil produced by the induced current is equal. At this time, the surface of the pipeline forms an electromagnetic equilibrium state and the detection coil does not generate an induced voltage. Figure 1b shows that when there is a crack in the surface of the pipeline, the magnetic and electrical permeability of the air at the crack is discontinuous with that of the surrounding pipeline. The magnetic flux and induced current will avoid the obstruction formed by the crack to meet the continuity. Most of the flux will flow through the bottom of the crack in the pipeline and there is still a part of the flux leaking into the air where the permeability is much lower. At the same time, the induced current flows around the crack and concentrates at both ends of the crack, causing an unequal amount of induced flux to penetrate into and out of the detection coil, disrupting the original electromagnetic equilibrium to form an electromagnetic field distortion, and then generating an induced voltage in the detection coil.

2.2. Sensor Mutual Inductance Model

The principle of the balanced-field electromagnetic technique is to detect the electromagnetic field distortion on the surface of the pipeline. The mutual inductance model of the balanced-field electromagnetic technique sensor is established using the method of impedance analysis [27] to further analyze the interaction between the pipeline and the balanced-field electromagnetic technique sensor. As the sensor consists of a pair of separate transceiver coils and the pipeline is a conductor, it can each be equated as a series connection of resistance and inductance that the excitation coil, detection coil, and the pipeline on the left and right sides of the center of the detection coil, forming circuits 1, 2, 3 and 4, respectively. U_I is the voltage of the excitation coil circuit and the induced voltage of the detection coil expressed as U_O, as shown in Figure 2. In the figure, M_{ij} is the mutual inductance coefficient between the circuits, I_i is the current of each circuit, R_i and L_i are the resistance and inductance of each circuit, respectively, i and j both are 1, 2, 3, and 4.

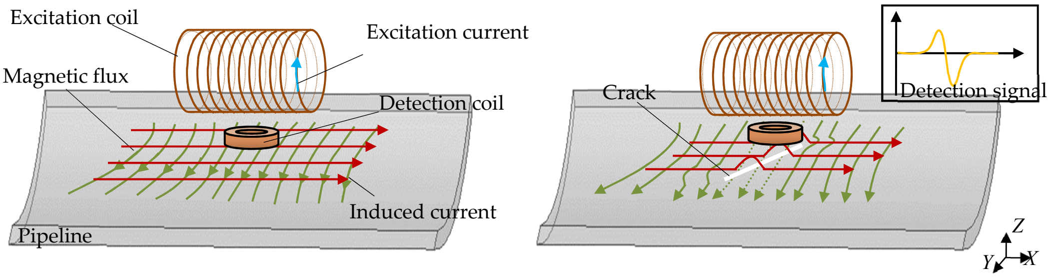

Figure 1. (**a**) Schematic diagram of electromagnetic distribution on the surface of the pipeline without defects; (**b**) schematic diagram of electromagnetic distribution on the surface of the pipeline with cracks.

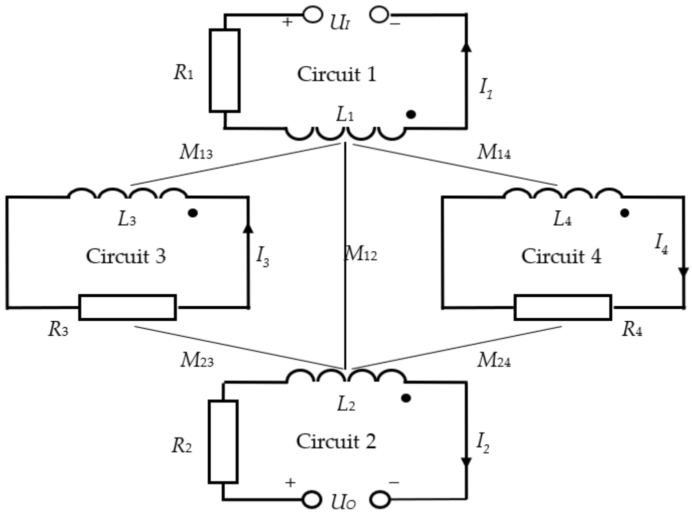

Figure 2. Mutual inductance model for detection of the balanced-field electromagnetic technique.

An expression for the mutual inductance model of the sensor in matrix form can be obtained according to the equivalence relations in Figure 2.

$$\begin{bmatrix} Z_1 & j\omega M_{12} & j\omega M_{13} & j\omega M_{14} \\ j\omega M_{21} & Z_2 & j\omega M_{23} & j\omega M_{24} \\ j\omega M_{31} & j\omega M_{32} & Z_3 & j\omega M_{34} \\ j\omega M_{41} & j\omega M_{42} & j\omega M_{43} & Z_4 \end{bmatrix} \begin{bmatrix} I_1 \\ I_2 \\ I_3 \\ I_4 \end{bmatrix} = \begin{bmatrix} U_I \\ U_O \\ 0 \\ 0 \end{bmatrix}, \tag{1}$$

where Z_i is the complex impedance of the circuit and is equal to the sum of the circuit resistance R_i and the inductive reactance $j\omega L_i$.

According to the Neumann formula [28], the mutual inductance coefficient M_{12} of circuit 1 and circuit 2 can be expressed as:

$$M_{12} = M_{21} = \frac{N_1 N_2 \mu_0}{4\pi} \oint_{l_1} \oint_{l_2} \frac{d\boldsymbol{l}_1 d\boldsymbol{l}_2}{\boldsymbol{r}}, \tag{2}$$

where N_1, N_2 are the number of excitation coil turns and the number of detection coil turns, respectively.μ_0 is the permeability of vacuum. $\boldsymbol{l}_1$, $\boldsymbol{l}_2$ are the equivalent current element for a single turn of the excitation coil and the equivalent current element for a single turn of the detection coil, respectively. $\boldsymbol{r}$ is the distance between the excitation coil current loop and the detection coil current loop.

The product of $d\boldsymbol{l}_1$ and $d\boldsymbol{l}_2$ is zero because the plane of the excitation coil is perpendicular to the plane of the detection coil and the distance between the excitation and detection coils is very close on the one hand and because $\boldsymbol{l}_1$ and $\boldsymbol{l}_2$ are distributed along the coil on the other. The mutual inductance coefficient M_{12} of circuit 1 and circuit 2 is zero, as a result. The above analysis shows from the perspective of mutual inductance that the orthogonal structure of the balanced-field electromagnetic technique sensor determines that the magnetic field generated by the excitation coil will not cause the detection coil to directly generate an induced voltage. Combined with Equation (1), the voltage of the excitation coil U_I and the voltage of the detection coil U_O can be obtained as:

$$U_I = Z_1 I_1 + j\omega M_{13} I_3 + j\omega M_{14} I_4, \tag{3}$$

$$U_O = Z_2 I_2 + j\omega M_{23} I_3 + j\omega M_{24} I_4, \tag{4}$$

According to Equation (4), it can be further analyzed that the generation principle of the detection signal of the balanced-field electromagnetic technique sensor. When the pipeline is without defects, the currents I_3 and I_4 in circuit 3 and circuit 4 are equal in magnitude and opposite in direction and there is no electromagnetic field distortion; therefore, I_2 is also zero. As a result, the detection coil output voltage U_O is zero. As the sensor moves through the pipeline with cracks, I_3 and I_4 are not equal and the electromagnetic balance is disturbed, causing I_2 to be non-zero, and thus U_O is not zero, with peaks at both edges of the crack.

2.3. Sensor Parameter Analysis

The extremely small size of the crack makes the generated signal very weak. To realize the crack detection more effectively, the parameters of the sensor can be adjusted to obtain a higher detection sensitivity. According to the principle of the balanced-field electromagnetic technique, the sensor outputs the electromagnetic field distortion caused by the crack as a voltage signal. At a certain crack size and excitation current, improving the sensitivity of the balanced-field electromagnetic technique sensor is to increase the detection coil output voltage as much as possible. According to the analysis in Section 2.2, the mutual inductance between the excitation coil circuit and the detection coil circuit is zero. Therefore, the analysis of the parameters affecting the detection voltage can be discussed from two aspects: the interaction between the excitation coil and the pipeline and the interaction between the detection coil and the pipeline.

The first is the interaction between the excitation coil and the pipeline. According to the principle of the balanced electromagnetic technique, at a certain crack size and excitation current I_1, the mutual inductance coefficient M_{1i} (i = 3,4) between the excitation coil circuit and the pipeline circuit increases so that the magnetic flux density on the surface of the pipeline also increases, correspondingly increasing the induced currents I_3 and I_4 on the surface of the pipeline. This in turn increases the degree of electromagnetic field distortion on the surface of the pipeline, causing the current I_2 in the detection coil circuit to also increase, thus increasing the detection voltage U_O. M_{1i} is expressed as:

$$M_{1i} = \frac{\mu_0 N_1}{4\pi} \oint_{l_1} \oint_{l_i} \frac{d\boldsymbol{l}_1 d\boldsymbol{l}_i}{\boldsymbol{r}_{1i}}, \tag{5}$$

It can be seen that the factors affecting the mutual inductance between the excitation coil circuit and the pipeline circuit are the number of turns of the excitation coil N_1, the distance $\boldsymbol{r}_{13}$ and $\boldsymbol{r}_{14}$ between the excitation coil and the pipeline. In addition, compared with the traditional balanced-field electromagnetic technique sensor without a magnetically conductive medium structure, the magnetic permeability in Equation (5) can be changed to direct more of the excitation magnetic field to the pipeline surface, thus affecting the mutual inductance between the excitation coil and the pipeline.

The next is the interaction between the detection coil and the pipeline. Similar to the analysis process for the excitation coil, the mutual inductance coefficient M_{2i} (i = 3,4) between the detection coil circuit and the pipeline circuit is expressed as:

$$M_{2i} = \frac{\mu_0 N_2}{4\pi} \oint_{l_2} \oint_{l_i} \frac{d\boldsymbol{l}_2 d\boldsymbol{l}_i}{\boldsymbol{r}_{2i}}, \tag{6}$$

The mutual inductance between the detection circuit and the pipeline circuit may be changed by adjusting the number of detection coil turns N_2, the distance between the detection coil and the pipeline $\boldsymbol{r}_{2i}$, and the detection coil containing the magnetically conductive medium, as shown in Equation (6). Moreover, the distance $\boldsymbol{r}_{1i}$ and $\boldsymbol{r}_{2i}$ between the excitation and detection coils and the pipeline form the lift-off distance of the sensor. As the above analysis has already shown that the extremely close distance between the excitation coil and the detection coil, as well as the spatially perpendicular position, means that the magnetic field generated by the excitation coil does not directly generate a voltage in the detection coil, it is possible to analyze the effect of the distance between the detection coil and the pipe on the sensitivity of the sensor only.

In summary, it can enable the sensor to achieve higher sensitivity and spatial resolution for more effective crack detection that adjusting the structural parameters of the excitation and detection coils and selecting the appropriate sensor lift-off distance.

3. Simulation of Sensor Parameters

Based on the analysis in Section 2, this section analyses the specific effects of adding a magnetically conductive medium to the coil, the number of coil turns and the sensor lift-off height on the sensitivity of the sensor by establishing a finite element simulation model to determine the sensor structural parameters of higher sensitivity. Considering that the depth of the crack is the indicator that mainly affects the failure of the pipeline in the evaluation of pipeline crack defects. Therefore, at a certain excitation current, the balanced-field electromagnetic technique sensor sensitivity S_n can be expressed as the ratio of the change in detection coil output voltage U_O to the change in crack depth d, as shown in Equation (7). According to the principle of the balanced-field electromagnetic technique, the output voltage is zero when there is no defect, so a higher sensor sensitivity is expressed as a larger detection voltage amplitude at the same crack depth.

$$S_n = \frac{\Delta U_O}{\Delta d} = \frac{U_O - 0}{d - 0} = \frac{U_O}{d} \tag{7}$$

3.1. Simulation Model

A 3D simulation model of pipeline crack detection was established by using COMSOL to analyze the influence of sensor parameters on the output voltage. Figure 3 shows the model, which includes air, excitation coil, detection coil, and local pipeline with cracks. The pipeline's material was X52 steel, which is typically used in long-distance oil and gas pipelines. The crack was parameterized at 90° to the detection direction (circumferential crack) and 0° to the detection direction (axial crack) to simulate the crack in the pipeline more realistically and make the analysis more applicable. Additionally, the crack depth was varied from 1 to 6 mm with an interval of 1 mm referring to the specification of the pipeline wall thickness in the standard of the American Petroleum Institute (API 5L), in order to analyze the response of the sensor to different depths of cracks. The material of the excitation coil and the detection coil were both set to copper, and their winding turns ranged from 100 to 700 turns, with an interval of 100 turns. The lift-off value between the detection coil and the pipeline surface was set from 1 to 7 mm with a 1 mm interval. A sinusoidal alternating voltage signal with a frequency of 1 kHz and a magnitude of 10 V was applied to the excitation coil to provide an alternating magnetic field for the model. Table 1 lists the individual model dimensional parameters.

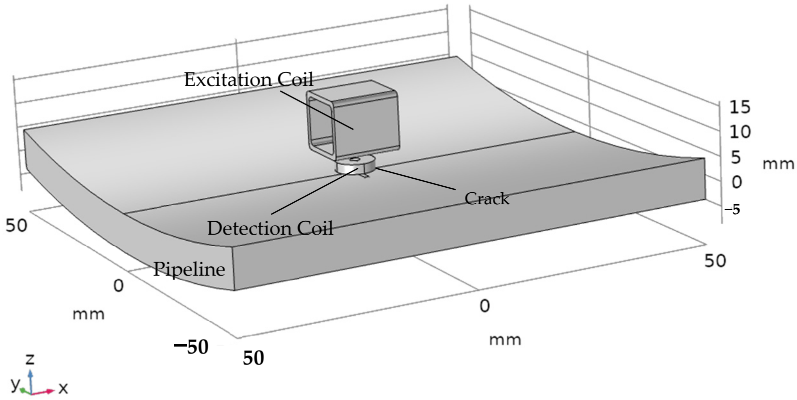

Figure 3. Simulation model of the balanced-field electromagnetic technique.

Table 1. Dimensional parameters of the simulation model.

Model	Inside Diameter (mm)	Outer Diameter (mm)	Length (mm)	Width (mm)	Depth (mm)
Excitation Coil	6	8	12	-	
Detection Coil	2	8	-	-	2
Pipeline	443	457	200	-	-
Crack	-	-	10	1	1 mm–6 mm
Air	-	600	-	-	-

3.2. Simulation Analysis of Sensor Structure Parameters

In order to specifically analyze the influence of the sensor structure parameters on the sensitivity, the results in this section are solved for in the Magnetic Field Interfaces under the Electromagnetic Fields in the AC/DC module of COMSOL. Ampere's law, Magnetic Insulation, and Initial Values are added to Magnetic Field Interfaces by default. The Free Tetrahedral mesh was used, where the maximum element size was 16.5 mm and the minimum element size was 1.2 mm. The pipeline directly below the detection coil was set with finer mesh to take into account the skin effect [29,30]. The specific structural parameters are analyzed below.

- Magnetically conductive medium

The magnetically conductive medium was added to the excitation and detection coils, respectively, to analyze the effect of the coil magnetically conductive medium on the output voltage, based on the model presented in Figure 3, and The material was Mn-Zn ferrite with a relative permeability of 2000. The magnetically conductive medium of the excitation coil is set in a U-shape to direct as much of the excitation magnetic field as possible to the surface of the pipeline so that the magnetic flux density on the surface of the pipeline increases. The magnetically conductive medium of the detection coil is set in a cylindrical shape to wind the detection coil more closely, as shown in Figure 4a. Figure 4b,c show the specific dimensions of the magnetically conductive medium.

The number of turns of the excitation coil and the detection coil is fixed at 400 and the sensor lift-off value is 1 mm. Three detection cases were simulated: no magnetically conductive medium, only magnetically conductive medium in the excitation coil, and magnetically conductive medium in both the excitation and detection coils, at a circumferential and axial crack depth of 3 mm. The sensor moved along the positive direction of the x-axis on the surface of the pipeline for detection, using the center of the crack as the origin and the coordinates (−20,0,0) and (20,0,0) as the start and end points, respectively. The simulation results are shown in Figure 5a,b. The peak-to-peak values of the signals in Figure 5a,b were extracted and plotted in Figure 5c to compare the amplitude of the detected signals more clearly.

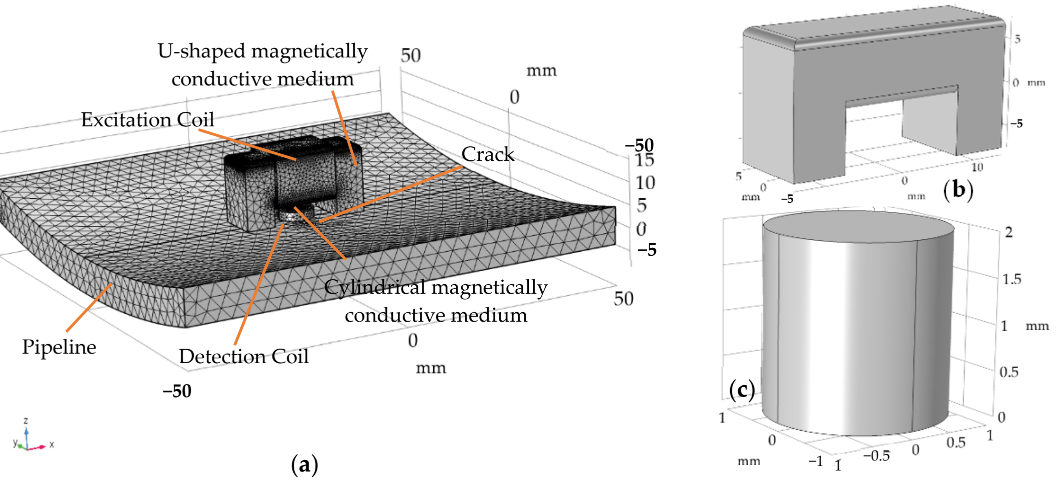

Figure 4. (**a**) Models with magnetically conductive medium; (**b**) dimensions of the magnetically conductive medium of the excitation coil; (**c**) dimensions of the magnetic conductive medium of the detection coil.

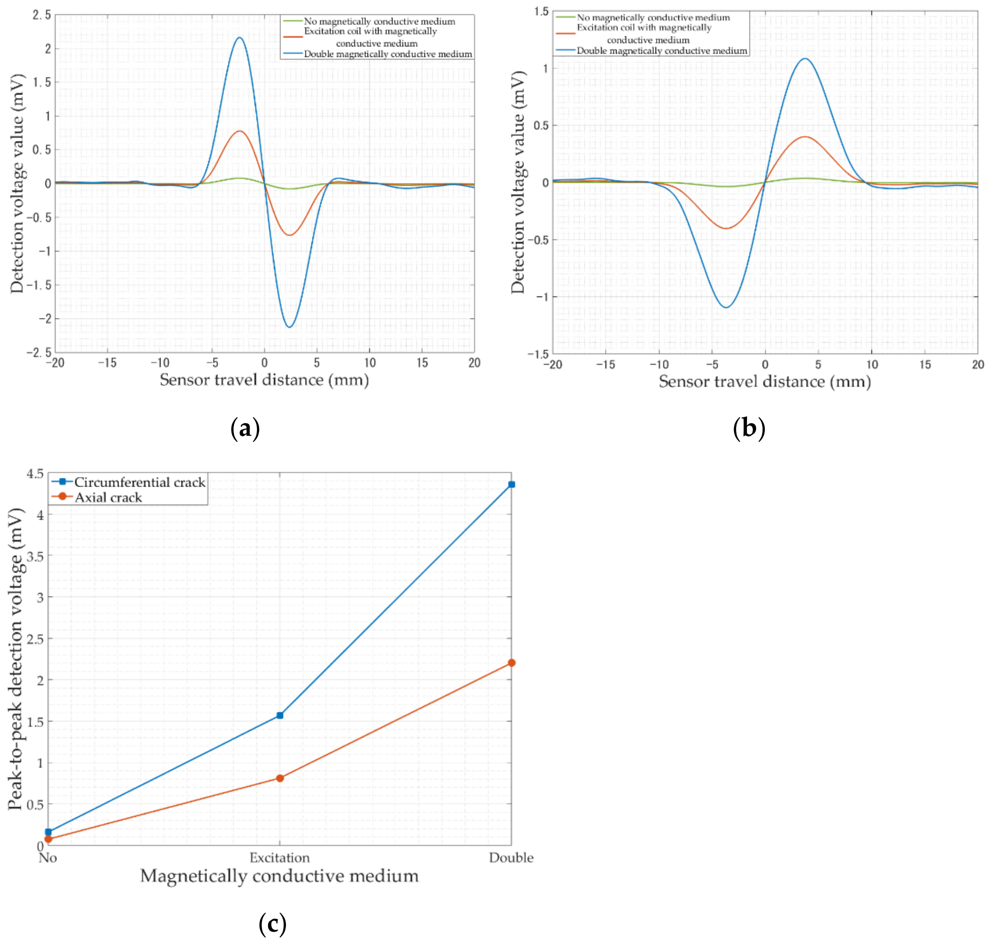

Figure 5. (**a**) Simulation voltage signal of circumferential crack; (**b**) simulation voltage signal of axial crack; (**c**) comparison of signal amplitude of detection voltage.

It can be seen that the addition of the magnetically conductive medium increases the detection voltage amplitude significantly compared to the no magnetically conductive medium, both for circumferential and axial crack detection. Compared to the no magnetically conductive medium, the detection voltage amplitude is 7.5-fold higher for excitation coils with the magnetically conductive medium and 21-fold higher for the double magnetically conductive medium. In addition, the detection voltage amplitude of the double magnetically conductive medium increases by 175% compared with the case where only the excitation coil contains the magnetically conductive medium, indicating that the magnetically conductive medium of the detection coil has a more obvious effect on increasing the detection voltage amplitude. The above analysis also shows that higher sensitivity can be achieved by using a structure in which both the excitation coil and detection coil contain the magnetically conductive medium.

- Number of the coil turns

Because the magnetically conductive medium has a positive effect on improving sensitivity, this part of the analysis is based on the model that both the excitation coil and detection coil contain the magnetically conductive medium to determine the number of the coil turns with high sensitivity. The detection effects were simulated and analyzed for the detection of circumferential and axial cracks of 1 to 6 mm depth with the different number of turns of excitation and detection coils, respectively. Firstly, the number of the detection coil turns was fixed at 400 and the number of the excitation coil turns was simulated from 100 to 700 with an interval of 100 turns. The peak-to-peak values of the detection voltage signal were extracted as shown in Figure 6a,b. It can be seen that the detection voltage amplitude grows as the crack depth increases, whether it is a circumferential crack or an axial crack. At a certain crack depth, the detection voltage amplitude increases with the increase in the number of the excitation coil turns and the rate of change is larger when the number of the excitation coil turns is 100 to 400 turns. The detection voltage amplitude decreases with the increase in the number of the excitation coil turns and the rate of change is smaller when the number of the excitation coil turns is 400 to 700 turns. The detection voltage amplitude is greatest when the number of the excitation coil turns is 400, which indicates that 400 turns may be chosen to achieve better sensitivity for the same depth of cracks.

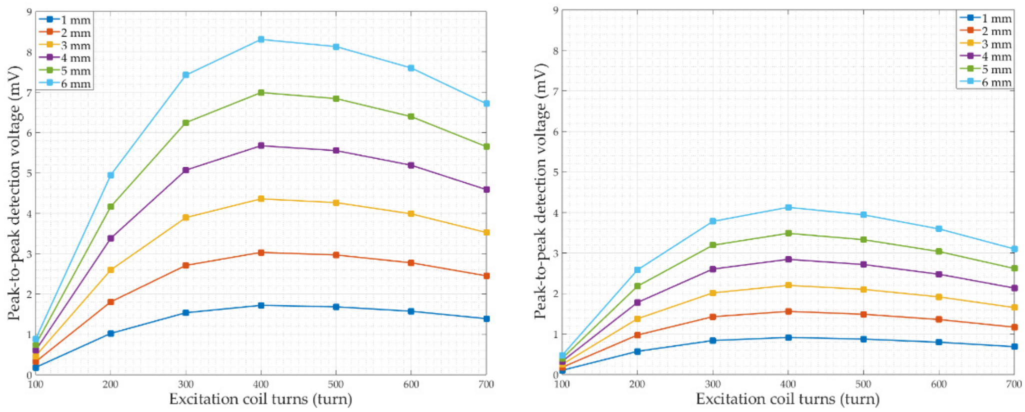

(**a**) (**b**)

Figure 6. (**a**) Detection voltage amplitude of circumferential cracks with different turns of excitation coil; (**b**) detection voltage amplitude of axial cracks with different turns of excitation coil.

Next, the number of the detection coil turns was analyzed. According to 2.3, the number of the excitation coil turns and the number of the detection coil turns have different effects on the sensitivity and the detection coil does not influence the excitation structure of the sensor. Therefore, the analysis of the optimal parameters of the detection coil can be carried out based on the optimal number of the excitation coil turns determined above. It was simulated for different turns of the detection coil that the detection of circumferential and axial cracks with a depth of 1 to 6 mm when the number of the excitation coil turns was fixed at 400 turns. The number of the detection coil turns was set from 100 to 700 turns with an interval of 100 turns and still extracted the peak-to-peak value of the detected voltage signal, as shown in Figure 7a,b. It can be seen from the figure that the detection voltage amplitudes for circumferential cracks and axial cracks both increase with the increase in the crack depth under the same number of the detection coil turns, indicating that the response to crack depth is also more obvious when the number of the detection coil turns is changed. At the same crack depth, the overall trend of the detected voltage amplitude increases with the increase in the number of the detection coil turns, and the rate of change at 100–400 turns is greater than that at 400–700 turns. In addition, the detection voltage amplitude tends to be stable when the number of the detection coil turns is 400–700 turns. Eventually, both the number of the detection coil turns and the excitation coil turns were determined to be 400 turns to achieve a higher detection voltage and sensor sensitivity, based on the aforementioned analysis and the impact of increasing the number of detection coil.

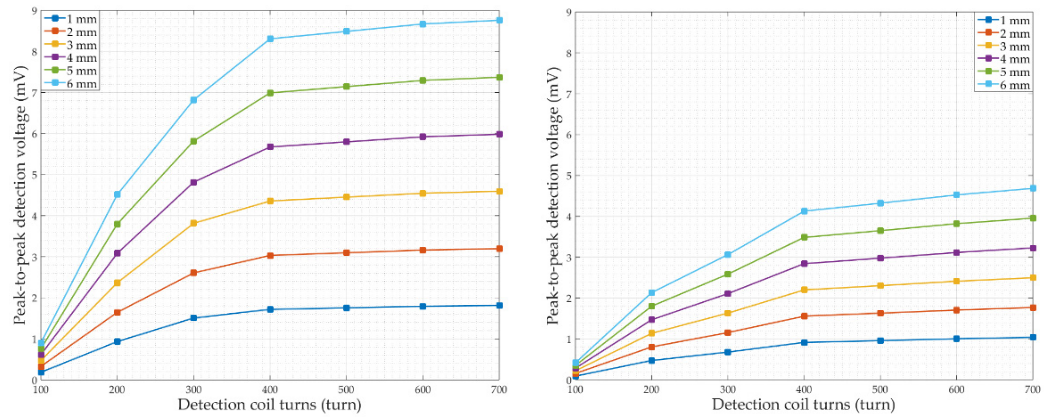

(**a**) (**b**)

Figure 7. (**a**) Detection voltage amplitude of circumferential cracks with different turns of detection coil; (**b**) detection voltage amplitude of axial cracks with different turns of detection coil.

- Lift-off value of the sensor

The lift-off value of the balanced-field electromagnetic technique sensor is the vertical distance between the detection coil and the pipeline. This paper analyzed the effect of lift-off values on the detection of circumferential and axial cracks of 1 to 6 mm in depth based on the simulation model containing a double magnetically conductive medium. The number of detection coil turns and excitation coil turns were fixed at 400 turns. Simulations were carried out for sensor lift-off values from 1 to 7 mm at 1 mm intervals, extracting the peak-to-peak values of the detection voltage as shown in Figure 8.

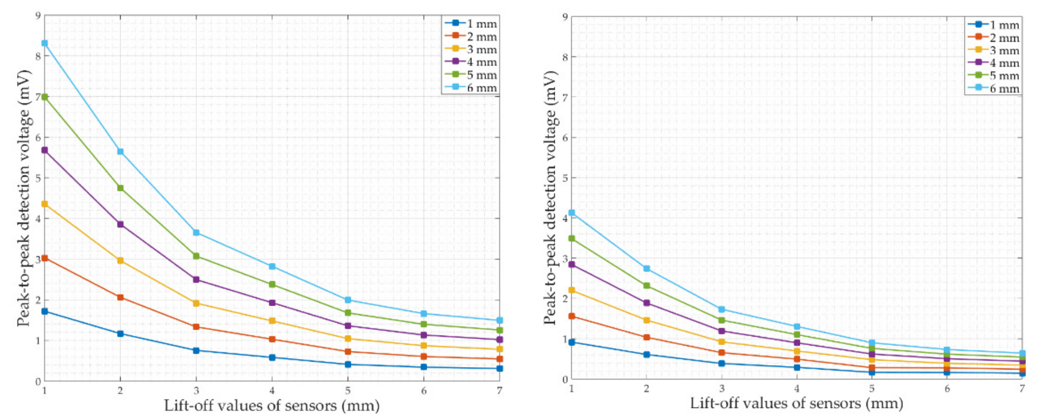

(**a**) (**b**)

Figure 8. (**a**) Detection voltage amplitudes of circumferential cracks with different lift-off values of the sensor; (**b**) detection voltage amplitudes of axial cracks with different lift-off values of the sensor.

It can be seen from the figure that the detection voltage amplitude increases with the increase in the crack depth, for each lift-off value. At the same crack depth, the detection voltage amplitude is the largest when the lift-off value is 1 mm and the detection voltage amplitude decreases in approximate exponential form and gradually approaches zero with the increase in the lift-off value of the sensor. It indicates that the smaller the lift-off value, the greater the mutual inductance between the detection coil and the pipeline. Due to the wear and tear of the actual application environment, it should be kept at a certain lift-off value during detection. The lift-off value of 1 mm was selected to ensure a higher detection sensitivity.

In summary, the balanced electromagnetic technique sensor is highly sensitive when the parameters analyzed above are adopted to design them and the detection voltage amplitude of the sensor varies with the change of depth of the crack. These parameters will be used later to create the sensor and carry out experiments. The specific design of the sensor parameters is as follows: adding a U-shaped excitation coil magnetic conductive medium and a cylindrical detection coil magnetic conductive medium to the traditional orthogonal coil structure; excitation coil and detection coil turns both are 400 turns, closely wound on the magnetic conductive medium; the sensor is kept at a lift-off value of 1 mm during detection.

4. Experiments and Analysis

In order to verify the detection capability and engineering practicality of the designed sensor, single-sensor experiments and pipeline pulling testing were carried out, respectively.

4.1. Single-Sensor Experiments

The balanced-field electromagnetic technique sensor was fabricated according to the parameters presented in Section 3 and built the balanced-field electromagnetic technique cracks detection experimental platform to verify the effectiveness of the designed sensor for the detection of cracks in real pipelines, as shown in Figure 9a. The detection experimental platform is composed of a detection system and a motion control system. The two systems are connected by using an elastic bracket to fix the sensor on the Z-axis of the three-axis sliding platform. The detection system is used to excite the sensor and to process and store the detection signal, and it consists of the balanced-field electromagnetic technique sensor, signal generator, lock-in amplifier, bandpass filter, and oscilloscope. The motion control system moves the sensor at a constant speed to simulate the process of the real pipeline inspection, and it consists of the three-axis sliding platform, stepper motor, motor controller, and computer. The experimental platform works on the following principle, as shown in Figure 9b: the computer sends a command to the motor controller to drive the stepper motor, and the stepper motor drives the three-axis sliding platform to move the sensor along the X-axis direction at a consistent speed. In the detection system, the signal generator generates a sine wave signal with a magnitude of 10 V and a frequency of 1 kHz, which is applied to the excitation coil of the balanced-field electromagnetic technique sensor and interacts with the pipeline to form an alternating electromagnetic field. The electromagnetic field distortion signal on the pipeline surface is picked up by the detection coil and processed through the bandpass filter, which is then input to the lock-in amplifier for processing. The output signal is displayed and stored by the oscilloscope.

The experimental objects were six X52 pipelines with a crack of different depths in the same dimensions as the simulation model. The pipeline cracks were machined using EDM technology, and they are all 6 mm in length, 0.5 mm in width, and 1 to 6 mm in depth at 1 mm intervals, as shown in Figure 10a. Due to the relative relationship between crack and detection direction, the circumferential crack and the axial crack detection were achieved by changing the direction of the pipeline while fixing the direction of sensor movement. S1 and S2 were positioned 20 mm to the left and right of the crack geometry center and used as the starting and ending points for the sensor movement, respectively. The sensor lift-off value was kept at 1 mm and detected at a speed of 40 mm/s. Figure 10b illustrates the movement path and detection direction of the sensor.

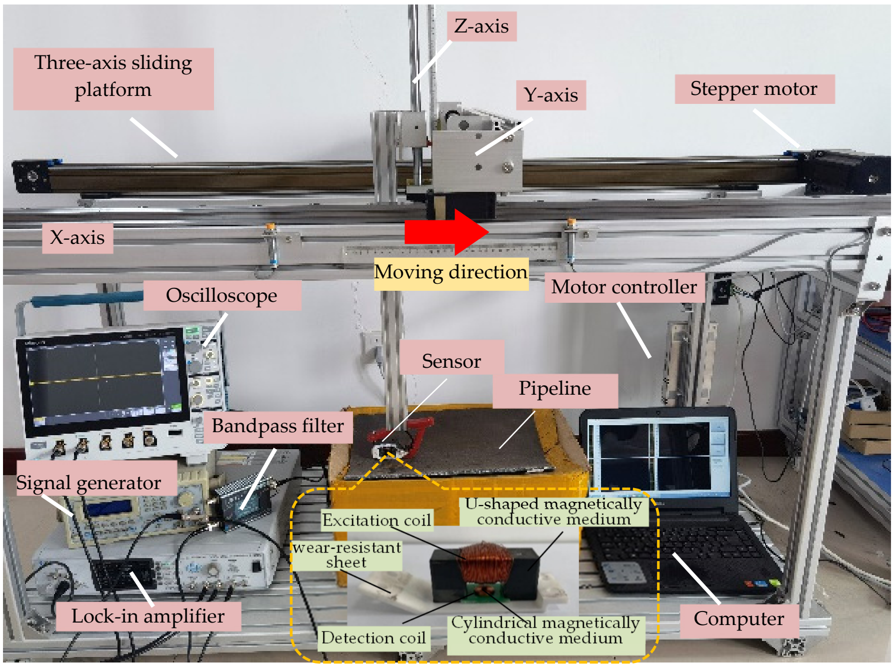

(**a**)

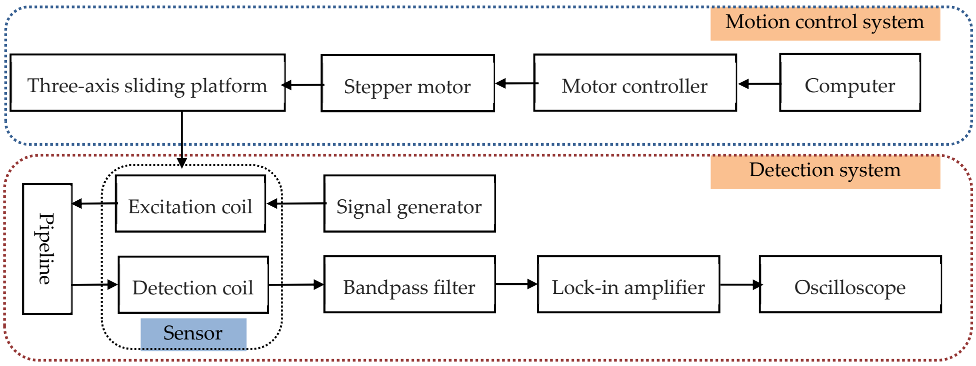

(**b**)

Figure 9. (**a**) Balanced-field electromagnetic technique crack detection experimental platform; (**b**) the working principle of the experimental platform.

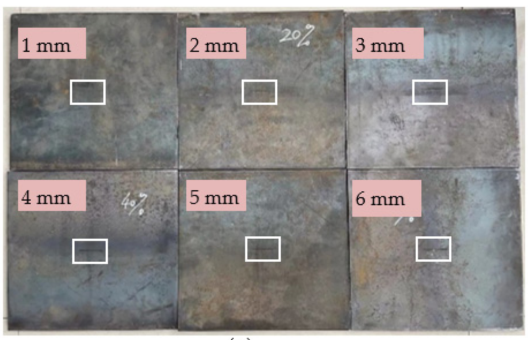

(**a**)

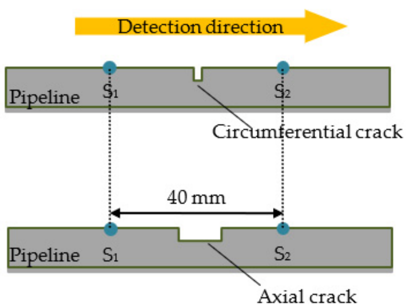

(**b**)

Figure 10. (**a**) Experimental pipelines with different depths of cracks; (**b**) schematic diagram of sensor movement path.

Following the path shown in Figure 10b, the pipeline is first placed vertically with the detection direction and then parallel with the detection direction for circumferential crack and axial crack detection of 1 mm–6 mm depth, respectively. To ensure the reliability of the test results, each set of experiments was repeated five times and the results were averaged, as shown in Figure 11. It can be seen from the two figures that the designed sensor has different output responses to cracks of different depths. The peak-to-peak value of the detection signal increases as the crack depth increases in both the circumferential and axial cracks. The signal for circumferential cracks is characterized by a peak followed by a valley, while the signal for axial cracks is characterized by a valley followed by a peak. The peak value and valley value of the signal are approximately equal for a fixed crack depth. The peak-to-valley spacing of the signal remains constant as the crack depth increases. The experimental results are consistent with the simulation analysis.

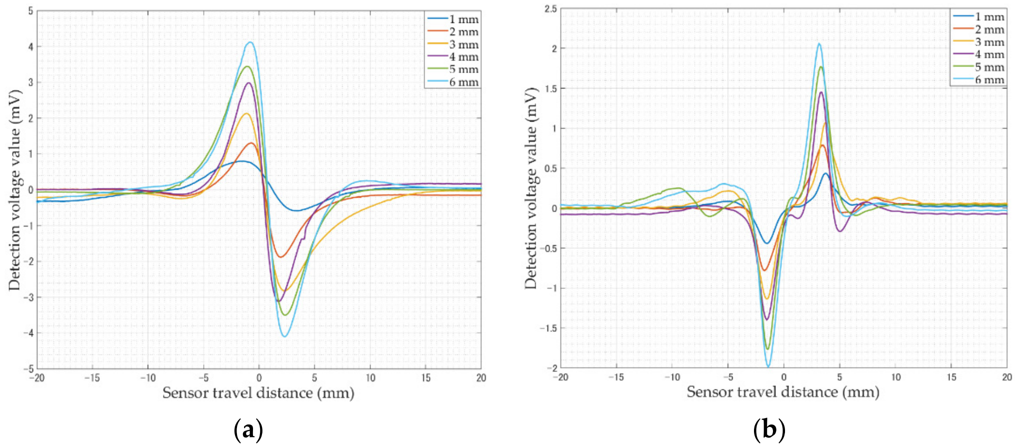

Figure 11. (**a**) Circumferential crack detection signal; (**b**) axial crack detection signal.

To further analyze the relationship between crack depth and detection signal amplitude, differenced the peak value and valley value of the detection signal for each depth crack to obtain the relationship between crack depth and amplitude for circumferential and axial cracks on the pipeline surface, respectively, as shown in Figure 12.

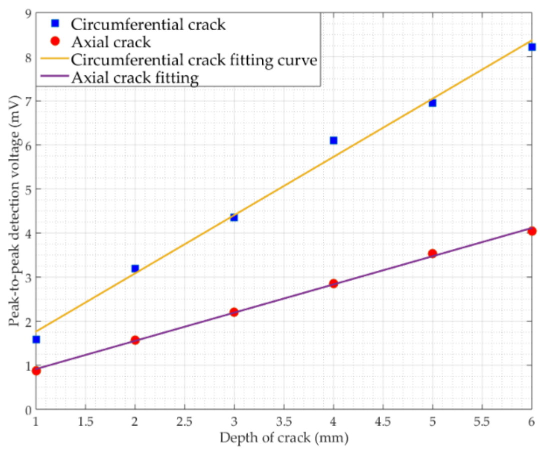

Figure 12. The relationship between the crack depth and the amplitude of the detection signal.

The figure illustrates that the detection signals of circumferential and axial cracks both grow in amplitude as crack depth increases, and the increasing trend is linear. This linear relationship is fitted as Equations (8) and (9). This linear numerical relationship also implies that the sensor is capable of quantifying the detection.

$$V_c = 1.321d + 0.4435, \tag{8}$$

$$V_a = 0.64d + 0.274, \quad (9)$$

where V_c is the circumferential crack detection signal amplitude. V_a is the axial crack detection signal amplitude and d is the crack depth.

In addition to fitting the relationship, the uncertainty of the test results was analyzed using statistical methods [31]. The random uncertainty σ for circumferential and axial cracks at each depth is expressed as:

$$\sigma = \pm\sqrt{\frac{\sum_{i=1}^{n}\left(\overline{V} - V_i\right)^2}{n(n-1)}}, \quad (10)$$

where n is the number of repeated experiments, n = 5. V_i is the voltage amplitude of a single detection, and $\overline{V}$ is the average value of the results of multiple detections at the same depth. The results of the uncertainty analysis are shown in Table 2.

Table 2. Uncertainty of experimental results.

Type of Cracks	Crack Depths (mm)	Results of Each Experiment (mV) 1	2	3	4	5	Average (mV)	σ
circumferential cracks	1	1.583	1.584	1.584	1.581	1.578	1.582	±0.00114
	2	3.194	3.19	3.193	3.191	3.187	3.191	±0.00122
	3	4.355	4.349	4.352	4.35	4.354	4.352	±0.00114
	4	6.105	6.101	6.106	6.107	6.101	6.104	±0.00127
	5	6.951	6.947	6.953	6.950	6.954	6.951	±0.00123
	6	8.225	8.223	8.221	8.22	8.226	8.223	±0.00114
axial cracks	1	0.880	0.875	0.873	0.878	0.879	0.877	±0.0013
	2	1.565	1.570	1.566	1.563	1.571	1.567	±0.00152
	3	2.205	2.210	2.211	2.206	2.208	2.208	±0.00114
	4	2.849	2.852	2.847	2.845	2.852	2.849	±0.00138
	5	3.535	3.538	3.534	3.537	3.541	3.537	±0.00122
	6	4.045	4.046	4.049	4.042	4.048	4.046	±0.00122

Next, it is analyzed the relationship δ between the detection voltage of circumferential cracks and axial cracks. It is obtained by extracting the rate of change k_c and k_a of V_c and V_a in Equations (8) and (9), respectively. As shown in Equation (11), the circumferential crack detection voltage amplitude for 1 mm–6 mm is approximately twice the amplitude of the axial crack detection voltage.

$$\delta = \frac{k_c}{k_a} = \frac{1.321}{0.64} \approx 2, \quad (11)$$

To analyze the sensitivity of the designed balanced-field electromagnetic technique sensor, the ratio was calculated of the change in crack detection voltage amplitude to the change in the crack according to Equation (7) for 1 mm–6 mm depth, respectively. The sensitivities of circumferential and axial cracks are shown in Figure 13.

It can be seen from the figure that the sensitivity of the designed sensor gradually decreases with the increase in the crack depth and tends to be stable. At a depth of 1 mm, the sensor's sensitivity is highest for both circumferential and axial cracks, with sensitivities of 1.76 and 0.87 mV/mm, respectively. The above findings show that the sensor has a high sensitivity to cracks of lesser depths. Because the deeper the crack are, the greater the feedback of the detection signal is and the easier it is to detect. Therefore, the higher sensitivity to smaller-depth cracks is more meaningful for practical applications.

4.2. Pipeline Pulling Testing

The pipeline pulling test was carried out to verify the engineering detection performance of the designed balanced-field electromagnetic technique sensor, as shown in

Figure 14a. A sensor unit composed of multiple balanced electromagnetic technique sensors was mounted on the PIG developed by the author's research team and the windlass was used to pull the PIG through the pipeline simulating the operation in the actual pipeline. PIG consists of the support structure, acquisition and storage unit, balanced-field electromagnetic technology sensor unit, odometer, and battery unit. Among them, the acquisition and storage unit is used to record all the detection data; the balanced-field electromagnetic technique sensors are staggered in two circles along the pipeline wall to form the detection unit; the odometer records the running distance; the support structure keeps the PIG close to the inner wall of the pipeline; the battery unit provides electricity for the PIG. For safety reasons, PIG all units are sealed and pressure-resistant.

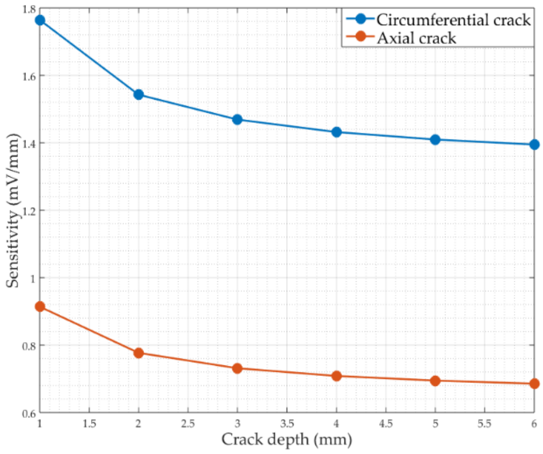

Figure 13. Sensitivity curve of the sensor.

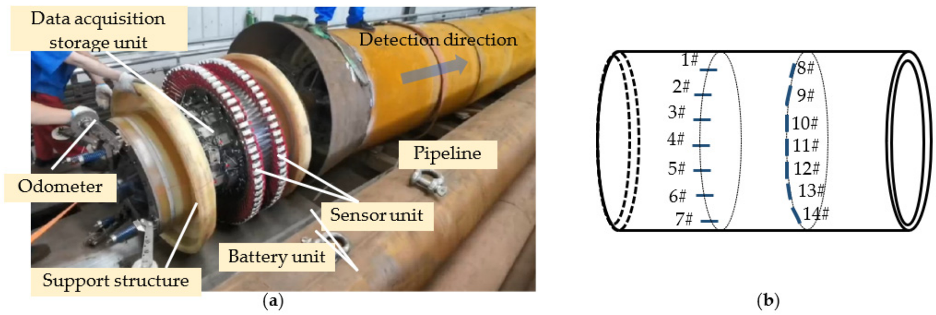

Figure 14. (**a**) Pipeline pulling test; (**b**) diagram of crack distribution.

The pipeline of the pulling test is still made of X52 material. The outer diameter of the pipeline is 1219 mm; the wall thickness is 20 mm; and the length is 2 m. The inner wall of the pipeline was prefabricated with circumferential and axial cracks of different depths. The crack lengths were all 100 mm and the widths were all 0.8 mm. The crack distribution is shown in Figure 14b and the crack sizes are shown in Table 3.

Table 3. Dimensional parameters of cracks.

Number	Depth (mm)	Crack Type	Number	Depth (mm)	Crack Type
1#	6	axial crack	8#	0.5	circumferential crack
2#	5		9#	1	
3#	4		10#	2	
4#	3		11#	3	
5#	2		12#	4	
6#	1		13#	5	
7#	0.5		14#	6	

The detection speed was set to 3 m/s and the PIG was pulled at one end of the pipeline in the detection direction shown in Figure 14a. The detection results are shown in Figure 15. The vertical axis in the figure represents the position along the circumferential direction of the pipeline, expressed in clock point, and one cycle of the pipeline is divided into 12 h. the horizontal axis represents the position along the axial axis of the pipeline (detection distance). It can be seen from the figure that the designed balanced-field electromagnetic technique sensor is still able to detect circumferential and axial cracks effectively at a speed of 3 m/s. In the case of dynamic pulling, the detection voltage amplitude also increases significantly with the increase in crack depth; the detection voltage amplitude is smallest at the crack depth of 0.5 mm; there is no distortion signal for the position without crack. Once again, it shows the clear differentiation in the response of the designed sensor to different crack depths.

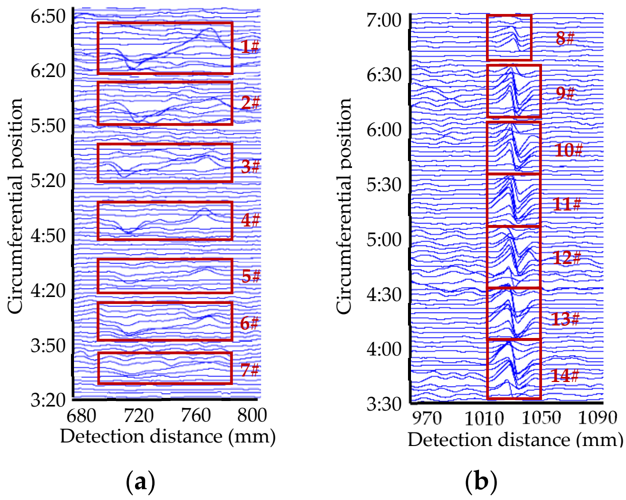

Figure 15. (**a**) Axial crack pulling test signal; (**b**) circumferential crack pulling test signal.

5. Discussion

According to the findings, the designed balanced-field electromagnetic technique sensor enables high-sensitivity detection of cracks in long-distance oil and gas pipelines and can be utilized in PIG for engineering inspection. It also has different responses for different depths of cracks. As there is no research on the balanced electromagnetic technique sensor, this section is compared with other sensors used in the field of in-line inspection of long-distance oil and gas pipelines. China Petroleum Pipeline Inspection Technology Co. developed an EMAT PIG, which can detect cracks with a depth greater than 3 mm at a speed of 2 m/s [32]. Figure 15 shows that at a speed of 3 m/s, the sensor designed in this paper can effectively detect cracks at a minimum depth of 0.5 m. In addition, ultrasonic detection sensors are difficult to detect cracks parallel to the propagation direction of ultrasonic waves [33,34]. Figures 11 and 15 both show that the designed sensor can detect both circumferential and axial cracks with high sensitivity in a single scan. Additionally, in principle, the balanced-field electromagnetic technique is capable of detecting cracks in arbitrary directions [25]. Eddy current testing sensors are effective for cracks in arbitrary direction; however, conventional eddy current is strongly affected by jitter interference in the vertical direction. Furthermore, the non-zero nature of eddy current detection allows for an output in the absence of cracks, which poses a challenge for crack discrimination [20,35]. Figures 11 and 15 and the analysis of the principle of the balanced-field electromagnetic technique both show that the designed sensor has no output voltage for no cracks and that the crack signal is clearly contrasted with the signal without cracks, which facilitates the detection of smaller cracks. In addition, Figure 13 also shows that the designed sensor has a high sensitivity to detect cracks at smaller depths, which is more relevant for practical applications.

Despite the better performance of the designed sensor compared to other sensors used on PIG, there are challenges in the engineering application of the actual pipeline. The balanced-field electromagnetic technique sensor relies on the detection coils to complete the crack signal pick-up. The structure of a single excitation coil and a single detection coil increases in size after adding a wear-resistant device, resulting in a corresponding increase in the spacing of the detection coils when multiple probes are arranged. Although it is possible to adopt a staggered arrangement of multiple circles to ensure full coverage of the inner wall of the pipeline along the circumference, this also increases the difficulty of aligning the data across multiple circles. In order to better cover the pipeline wall, it is possible to adopt the structure of a single excitation coil and multiple detection coils and the total sensitivity of the multiple detection coils is analyzed. This structure is advantageous for adapting to the detection of pipelines with different pipeline diameters.

In addition, the results of this study provide an effective method for the high-sensitivity detection of inner wall cracks in arbitrary directions of long-distance oil and gas pipelines. However, the detection of buried cracks is more difficult due to the skin effect, which can be investigated in terms of the relationship between the electromagnetic field strength and the skin depth as well as the excitation parameters of the sensor. This is practical for perfecting the ability of the balanced-field electromagnetic technique to in-line inspection cracks of long-distance oil and gas pipelines.

6. Conclusions

According to the requirement of sensor sensitivity for crack detection of long oil and gas pipelines, this paper designs a balanced-field electromagnetic technique sensor which can detect both circumferential and axial cracks and is used for in-line inspection of pipelines. The research results show that when it is lifted 1 mm away from the pipeline surface and the speed is within 3 m/s, the sensor can detect circumferential and axial cracks with high sensitivity in the pipeline with a depth of 0.5–6 mm; a single sensor or the form of a sensor array formed on the PIG have obvious differentiation for the amplitude of crack detection voltage at different depths; the response of a single sensor to the crack depth is: the amplitude of detection voltage increases linearly with the increase in crack depth, and the amplitude of circumferential crack detection voltage at the same depth is twice that of axial crack, which provides a reference for further quantifying the crack depth. The designed sensor has different sensitivity to circumferential cracks and axial cracks, and has higher sensitivity to smaller cracks. The sensitivity of circumferential and axial cracks at 1 mm depth can reach 1.76 and 0.87 mV/mm, respectively. Future work will further the study of the engineering adaptability of sensors.

Author Contributions: Conceptualization, J.L. and W.Z.; methodology, J.L. and W.Z.; software, J.L.; validation, J.L. and W.Z.; formal analysis, J.L. and W.Z.; investigation, J.L. and W.Z.; resources, L.Y.; data curation, J.L. and W.Z.; writing—original draft preparation, J.L.; writing—review and editing, J.L. and W.Z.; visualization, J.L.; supervision, L.Y.; project administration, L.Y. and B.L.; funding acquisition, B.L. All authors have read and agreed to the published version of the manuscript.

Funding: This research was funded by the National Natural Science Foundation of China (Grant No.61871450).

Institutional Review Board Statement: Not applicable.

Informed Consent Statement: Not applicable.

Data Availability Statement: Not applicable.

Acknowledgments: The study was approved by the Shenyang University of Technology.

Conflicts of Interest: The authors declare no conflict of interest.

References

1. Provornaya, I.V.; Filimonova, I.V.; Mishenin, M.V.; Dzyuba, Y.A.; Chebotareva, A.V. The influence of the pipeline system on the socio-economic development of oil and gas regions. *IOP Conf. Ser. Earth Environ. Sci.* **2021**, *823*, 012021. [CrossRef]
2. Zakikhani, K.; Nasiri, F.; Zayed, T. A review of failure prediction models for oil and gas pipelines. *J. Pipeline Syst. Eng. Pract.* **2020**, *11*, 03119001. [CrossRef]
3. Ben Seghier, M.E.A.; Höche, D.; Zheludkevich, M. Prediction of the internal corrosion rate for oil and gas pipeline: Implementation of ensemble learning techniques. *J. Nat. Gas Sci. Eng.* **2022**, *99*, 104425. [CrossRef]
4. Wasim, M.; Djukic, M.B. External corrosion of oil and gas pipelines: A review of failure mechanisms and predictive preventions. *J. Nat. Gas Sci. Eng.* **2022**, *100*, 104467. [CrossRef]
5. Quej-Ake, L.M.; Rivera-Olvera, J.N.; Domínguez-Aguilar, Y.D.; Avelino-Jiménez, I.A.; Garibay-Febles, V.; Zapata-Peñasco, I. Analysis of the physicochemical, mechanical, and electrochemical parameters and their impact on the internal and external scc of carbon steel pipelines. *Materials* **2020**, *13*, 5771. [CrossRef]
6. Feng, Q.; Li, R.; Nie, B.; Liu, S.; Zhao, L.; Zhang, H. Literature Review: Theory and application of in-line inspection technologies for oil and gas pipeline girth weld defection. *Sensors* **2017**, *17*, 50. [CrossRef]
7. Ambati, P.; Raj, K.M.S.; Joshuva, A. A review on pipeline inspection robot. *AIP Conf. Proc.* **2020**, *2311*, 060002. [CrossRef]
8. Ma, Q.; Tian, G.; Zeng, Y.; Li, R.; Song, H.; Wang, Z.; Gao, B.; Zeng, K. Pipeline in-line inspection method, instrumentation and data management. *Sensors* **2021**, *21*, 3862. [CrossRef]
9. Song, H.; Yang, L.; Liu, G.; Tian, G.; Ona, D.; Song, Y.; Li, S. Comparative analysis of in-line inspection equipments and technologies. *IOP Conf. Ser. Mater. Sci. Eng.* **2018**, *382*, 032021. [CrossRef]
10. Bubenik, T. Electromagnetic methods for detecting corrosion in underground pipelines: Magnetic flux leakage (MFL). In *Underground Pipeline Corrosion*; Orazem, M.E., Ed.; Woodhead Publishing: Sawston, UK, 2014; pp. 215–226.
11. Durai, M.; Lin, Z.-Q.; Lan, C.-W.; Chang, H.; Peng, C.-C. Study of defects in the petrochemical storage tank floor using the magnetic flux leakage (MFL) technique. *J. Fail. Anal. Prev.* **2022**, *22*, 807–814. [CrossRef]
12. Dobmann, G.; Barbian, O.A.; Willems, H. State of the art of in-line nondestructive weld inspection of pipelines by ultrasonics. *Russ. J. Nondestr. Test.* **2007**, *43*, 755–761. [CrossRef]
13. Da, Y.; Dong, G.; Shang, Y.; Wang, B.; Liu, D.; Qian, Z. Circumferential defect detection using ultrasonic guided waves. *Eng. Comput.* **2020**, *37*, 1923–1943. [CrossRef]
14. Yang, L.; Zhang, J.; Xing, Y.; Gao, S.; Xie, Z.; Fu, H. Development of a biaxial grid-coil-type electromagnetic acoustic transducer. *Meas. Sci. Technol.* **2020**, *32*, 025102. [CrossRef]
15. Nakamura, N.; Ashida, K.; Takishita, T.; Ogi, H.; Hirao, M. Inspection of stress corrosion cracking in welded stainless steel pipe using point-focusing electromagnetic-acoustic transducer. *NDT E Int.* **2016**, *83*, 88–93. [CrossRef]
16. Salzburger, H.-J.; Niese, F.; Dobmann, G. EMAT pipe inspection with guided waves. *Weld. World* **2012**, *56*, 35–43. [CrossRef]
17. Zhou, D.; Chang, X.; He, Y.; Wang, H.; Cao, P.; Yang, L. Influence of key factors on eddy current testing sensitivity and monotonicity on subsurface depth for ferromagnetic and non-ferromagnetic materials. *Sens. Actuators A Phys.* **2018**, *278*, 98–110. [CrossRef]
18. Piao, G.; Guo, J.; Hu, T.; Deng, Y.; Leung, H. A novel pulsed eddy current method for high-speed pipeline inline inspection. *Sens. Actuators A Phys.* **2019**, *295*, 244–258. [CrossRef]
19. She, S.; Chen, Y.; He, Y.; Zhou, Z.; Zou, X. Optimal design of remote field eddy current testing probe for ferromagnetic pipeline inspection. *Measurement* **2021**, *168*, 108306. [CrossRef]
20. Faraj, M.A.; Samsuri, F.; AbdAlla, A.N.; Rifai, D.; Ali, K.; Al-Douri, Y. Investigate the effect of lift-off on eddy current signal for carbon steel plate. *MATEC Web Conf.* **2018**, *225*, 06005. [CrossRef]
21. Newton, K.; Martin, R.; Topp, D.J.I. The ACFM technique and its application to the inspection of oil and gas installations. *Insight* **1994**, *36*, 422–425.
22. Li, W.; Xin, A.Y.; Chen, G.; Yin, X.; Ge, J.; Kong, Q.; Zhang, Y.; Wu, Y. Detection of cracks in metallic objects by arbitrary scanning direction using a double u-shaped orthogonal ACFM probe. *Mater. Trans.* **2016**, *57*, 608–612. [CrossRef]
23. Sun, L.; Zhao, S.; Shen, Y.; Wang, J.; Gao, J. A performance improved ACFM-TMR detection system with tradeoff denoising algorithm. *J. Magn. Magn. Mater.* **2021**, *527*, 167756. [CrossRef]
24. Yuan, X.A.; Li, W.; Chen, G.; Yin, X.; Ge, J.; Yang, W.; Liu, J.; Ma, W. Inner circumferential current field testing system with TMR sensor arrays for inner-wall cracks inspection in aluminum tubes. *Measurement* **2018**, *122*, 232–239. [CrossRef]
25. Yang, L.; Zheng, W.; Li, J.; Gao, S.; Liu, B. Full-angle detection method of pipeline crack based on balanced electromagnetic technology. *Chin. J. Sci. Instrum.* **2021**, *42*, 103–112. [CrossRef]
26. Yang, L.; Zheng, W.; Gao, S.; Liu, B. Steel plate crack defect detection method based on balanced electromagnetic technology. *Chin. J. Sci. Instrum.* **2020**, *41*, 196–203. [CrossRef]
27. Luloff, M.S.; Desjardins, D.; Morelli, J.; Krause, T.W. Solution for a transmit-receive eddy current probe above a layered planar conductive structure. *NDT E Int.* **2018**, *96*, 1–8. [CrossRef]
28. Desjardins, D.; Krause, T.W.; Clapham, L. Transient response of a driver-pickup coil probe in transient eddy current testing. *NDT E Int.* **2015**, *75*, 8–14. [CrossRef]
29. Kubiczek, K.; Kampik, M. Highly accurate and numerically stable computations of double-layer coaxial waveguides. *Eng. Comput.* **2019**, *36*, 1384–1399. [CrossRef]

30. Tabei, B.; Ametani, A.; Gole, A.M.; Kordi, B. Quasi-analytical calculation of frequency-dependent resistance of rectangular conductors considering the edge effect. *Energies* **2022**, *15*, 503. [CrossRef]
31. Dhakal, P.; Adhikari, M.; Thapa, B.S.; Kayastha, A.; Sapkota, P.; Dahal, D.R. Uncertainty evaluation of efficiency measurement in laboratory conditions. *J. Phys. Conf. Ser.* **2020**, *1608*, 012007. [CrossRef]
32. Zang, Y.; Jin, Y.; Chen, C.; Di, Q.; Zhao, X. Design of mechanical structure of crack detector for pipeline based on the magnetostrictive effect. *Oil Gas Storage Transp.* **2015**, *34*, 775–778.
33. Caleyo, F.; Alfonso, L.; Espina-Hernández, J.H.; Hallen, J.M. Criteria for performance assessment and calibration of in-line inspections of oil and gas pipelines. *Meas. Sci. Technol.* **2007**, *18*, 1787–1799. [CrossRef]
34. Liu, J.; Liu, S.; Jin, L.; Zhang, C.; Yang, Q. Simulation and experiment of orthogonal shear waves with electromagnetic acoustic transducer for thickness measurement and crack detection. *Trans. China Electrotech. Soc.* **2022**, *37*, 2686–2697. [CrossRef]
35. Fu, Y.; Lei, M.; Li, Z.; Gu, Z.; Yang, H.; Cao, A.; Sun, J. Lift-off effect reduction based on the dynamic trajectories of the received-signal fast Fourier transform in pulsed eddy current testing. *NDT E Int.* **2017**, *87*, 85–92. [CrossRef]